JOC Article

Probing Molecular Recognition in the Solid-State by Use of an Enolizable Chromophoric Barbituric Acid

Ina Bolz,[†] Chulsoon Moon,[‡] Volker Enkelmann,[‡] Gunther Brunklaus,[‡] and Stefan Spange*[,†]

Institut für Chemie, Technische Universität Chemnitz, D-09107 Chemnitz, Germany, and Max-Planck-Institut für Polymerforschung, Postfach 3148, D-55021 Mainz, Germany

stefan.spange@chemie.tu-chemnitz.de; brunklaus@mpip-mainz.mpg.de

Received July 19, 2007

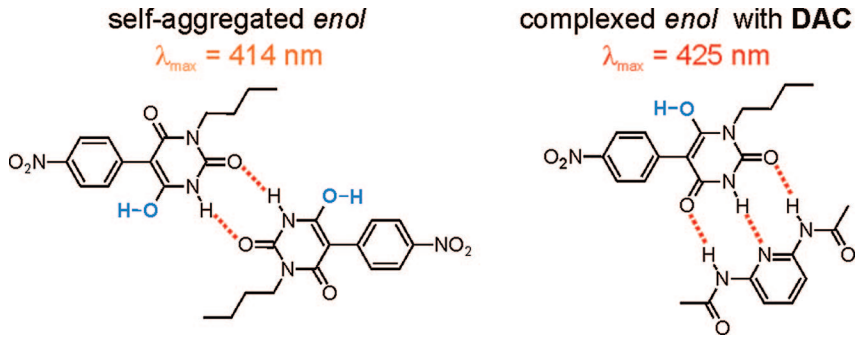

Complex formation of the enolizable chromophor 1-*n*-butyl-5-(4-nitrophenyl)barbituric acid **1** with multiple binding sites for supramolecular assemblies and its corresponding adducts produced with the Proton Sponge (1,8-bis(dimethylamino)naphthalene, **PS**) and the adenine-mimetic 2,6-diacetamidopyridine (**DAC**) have been studied by means of solid-state proton NMR spectroscopy under fast magic-angle spinning, X-ray analysis, and UV/vis spectroscopy. Both NMR data and X-ray results reveal that the *enolic* chromophor undergoes self-aggregation to hydrogen-bonded dimers which are involved in stacked arrangements. Depending on the nature of the added base, this dimeric assembly is preserved in the formed *enolate* anion but can be broken in the presence of complementary hydrogen-bonding pattern leading to supramolecular complexes. Molecular recognition of these structural different bases significantly influences the chromophoric π-system of **1**.

I. Introduction

Artificial chromophoric receptors for biologically active molecules have attracted considerable attention from the viewpoint of molecular recognition.[1,2] In particular, interactions mediated by hydrogen-bonding play an important role in both chemical and biological systems.[3] Barbiturates are important members of the pyrimidine family and show very selective affinities at binding adenine or its derivatives, thereby yielding strongly hydrogen-bonded complexes.[4] However, the observed biological activity of barbiturates is mainly attributed to tautomerism, acid−base equilibriums, and to the nature of their substituents.[5] Recently, it has been shown that related Merocyanine dyes create new self-assembled structures[6] or are effective sensitizers with interesting photophysical properties.[7] More importantly, such dyes exhibit hydrogen-bonding patterns with an ADA sequence (A = hydrogen bond acceptor site,

[†] Institut für Chemie, Technische Universität Chemnitz.

[‡] Max-Planck-Institut für Polymerforschung. To whom correspondence pertaining to NMR and X-ray structure analyses should be addressed.

(1) For recent reviews, see: (a) Demeunynck, M., Bailly, C., Wilson, W. D., Eds. *DNA and RNA binders*; Wiley-VCH, Weinheim, 2003. (b) De Silva, A. P.; Gunaratne, H. Q. N.; Gunnlaugsson, T.; Huxley, A. J. M.; McCoy, C. P.; Rademacher, J. T.; Rice, T. E. *Chem. Rev.* **1997**, *97*, 1515–1566, and references cited therein.

(2) For some selected recent publications, see: Liu, J.; Lu, Y. *Angew. Chem.* **2006**, *118*, 96−100; *Angew. Chem., Int. Ed.* **2006**, *45*, 90−94. (b) Sando, S.; Abe, H.; Kool, E. T. *J. Am. Chem. Soc.* **2004**, *126*, 1081–1087. (c) Okamoto, A.; Tainaka, K.; Saito, K.-i. N. I. *J. Am. Chem. Soc.* **2005**, *127*, 13128–13129. (d) Thompson, K. C.; Miyake, N. *J. Phys. Chem. B* **2005**, *109*, 6012–6019, and references cited therein.

(3) Paulini, R.; Müller, K.; Diederich, F. *Angew. Chem.* **2005**, *117*, 1820−1839; *Angew. Chem., Int. Ed.* **2005**, *44*, 1788−1805.

(4) (a) Kyogoku, Y.; Lord, R. C.; Rich, A. *Nature* **1968**, *218*, 69–72. (b) Voet, D.; Rich, A. *J. Am. Chem. Soc.* **1972**, *94*, 5888–5891.

(5) Zuccarello, F.; Buemi, G.; Gandolfo, C.; Contino, A. *Spectrochim. Acta A* **2003**, *59*, 139–151.

(6) (a) Bohanon, T. M.; Denzinger, S.; Fink, R.; Paulus, W.; Ringsdorf, H.; Weck, M. *Angew. Chem.* **1995**, *107*, 102−104; *Angew. Chem., Int. Ed.* **1995**, *34*, 58−60. (b) Bohanon, T. M.; Caruso, P.-L.; Denzinger, S.; Fink, R.; Möbius, D.; Paulus, W.; Preece, J. A.; Ringsdorf, H.; Schollmeyer, D. *Langmuir* **1999**, *15*, 177–184.

10.1021/jo800598z CCC: $40.75 © 2008 American Chemical Society
Published on Web 06/10/2008

SCHEME 1. *Keto*−*Enol* Tautomerism of 1 Producing Hydrogen-Bonding Patterns (A = Hydrogen Bond Acceptor Site, D = Hydrogen Bond Donor Site)[a]

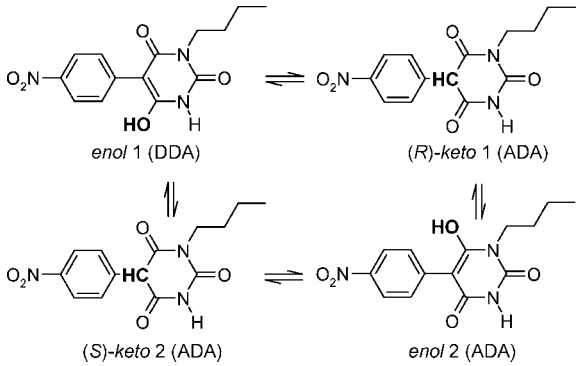

[a] Two different *enol* forms with either vicinal or opposed OH and NH protons are possible.

D = hydrogen bond donor site) suitable for selective binding to bases offering a complementary DAD pattern. Merocyanine dyes which contain the barbituric acid moiety as an electron-withdrawing group are well established in the literature.[6–8] Due to the barbituric acid moiety being negatively polarized in merocyanine-type dyes their UV/vis absorption band is affected by acids rather than by proton acceptors, which makes them unsuitable for the recognition of bases with ADA pattern or related molecules.[8]

Therefore, in our conceptual development the barbituric acid moiety should be an electron-donating substituent and has to be linked to chromophores which bear electron-withdrawing substituents. These requirements are accomplished, if the barbituric acid is directly linked at the C5-position to a chromophoric system under retention of an acid proton suitable to undergo *keto*−*enol* equilibriums. However, these structurally simple barbiturates are still not established in the literature which is assigned to the nontrivial structure determination.[9] The occurrence of the tautomeric forms offers two different hydrogen-bonding patterns ADA and DDA, respectively. Furthermore, aggregate formation complicates a clear structure assignment of those dyes even in the pure form. Therefore, the detailed knowledge of the structural versatility of enolizable barbituric acid dyes is very important in order to construct novel types of UV/vis probes for molecular recognition.

In this paper, we report on the synthesis and solid-state structure of the enolizable chromophor 1-*n*-butyl-5-(4-nitrophenyl)barbituric acid **1** that features adjustable hydrogen-bonding properties. The prototropic tautomerism of this dye facilitates an adjustment to complementary bases containing a DDA or ADA sequences (Scheme 1).

The switching between the two principle tautomeric forms of **1** (*keto*1/*keto*2 or *enol*1/*enol*2, cf. Scheme 1) is associated with dramatic changes in the extent of π-conjugation. The *enol* substituent contributes to a push−pull system due to the *para* conjugation with the nitro group, while the *keto* substituent belongs to a common nitro-substituted aromatic system. Thus, externally induced formation of the *enol*1 or *enol*2 form should cause a significant bathochromic shift in the UV/vis spectrum. In contrast to the established Merocyanine dyes, the enolizable barbituric acid serves as a (+M)-substituent which is of importance for the construction of chromophoric probes relating to this type of compounds that are still not established for probing molecular recognition. However, the possible occurrence of both tautomeric forms as well as molecular adducts complicates a clear assignment of observed UV/vis absorption spectra to a well-defined molecular structure.

Therefore, we have investigated the solid-state structures of the corresponding assemblies of **1** with the Proton Sponge **PS** and the adenine-mimetic base 2,6-diacetamidopyridine **DAC** to identify whether mere salt formation occurs or rather genuine supramolecular complexes are built. The balance between them is dependent on both the presence of a suitable hydrogen-bonding pattern of the base and its basicity strength,[10] e.g., an association of nucleobases with synthetic ligands like **DAC** mediated by hydrogen bonds has been a longstanding focus of supramolecular chemistry.[11] Proton-transfer reactions of Brønsted acids in the presence of **PS** have been widely studied.[12] The synergism of the two effects and its influence on the complex (or salt) structures of **1** with different bases is a further objective of this work. Since various molecular structures can contribute to the UV/vis response caused by the molecular recognition, a thorough investigation of the solid-state structures is required to demonstrate the versatile bonding potential of this new type of compound toward those structurally different bases.

In order to derive the structure of the various compounds, we employed both single-crystal X-ray analysis and advanced solid-state NMR spectroscopy, which in recent years has shown to be a versatile and powerful tool for the characterization of materials.[13,14] In particular, information about hydrogen-bonding

(7) (a) Würthner, F.; Yao, S.; Debaerdemaeker, T.; Wortmann, R. *J. Am. Chem. Soc.* **2002**, *124*, 9431–9447. (b) Würthner, F.; Yao, S. *J. Org. Chem.* **2003**, *68*, 8943–8949. (c) Würthner, F. W. *Chem. Commun.* **2004**, 1564–1579.

(8) (a) Rezende, M. C.; Campodonico, P.; Abuin, E.; Kossanyi, J. *Spectrochim. Acta A* **2001**, *57*, 1183–1190. (b) Kulinich, A. V.; Derevyanko, N. A.; Ishchenko, A. A. *Russ. J. Gen. Chem.* **2006**, *76*, 1441–1457. (Engl.Transl.)

(9) (a) Braun, H.-J. Semadeni, P. A. Ger. 1999, DE 19728389 C1. (b) Bolz, I.; May, C.; Spange, S. *Arkivoc* **2007**, *iii*, 60–67. (c) Bolz, I.; May, C.; Spange, S. *New J. Chem.* **2007**, *31*, 1568–1571.

(10) Kaljurand, I.; Kütt, A.; Sooväli, L.; Rodima, T.; Mäemets, V.; Leito, I.; Koppel, I. A. *J. Org. Chem.* **2005**, *70*, 1019–1028.

(11) For some selected recent publications, see: (a) Jorgensen, W. L.; Pranata, J. *J. Am. Chem. Soc.* **1990**, *112*, 2008–2010. (b) Yu, L.; Schneider, H.-J. *Eur. J. Org. Chem.* **1999**, 1619–1625. (c) Zimmerman, S. C.; Corbin, P. C. *Struct. Bonding (Berlin)* **2000**, *96*, 63–94. (d) Rotello, V. M. *Curr. Org. Chem.* **2001**, *5*, 1079–1090, and references cited therein.

(12) (a) Staab, H. A.; Saupe, T. *Angew. Chem.* **1988**, *100*, 895−909; *Angew. Chem., Int. Ed.* **1988**, *27*, 865−879. (b) Alder, R. W. *Chem. Rev.* **1989**, *89*, 1215–1223. (c) Llamas-Saiz, A. L.; Foces-Foces, C.; Elguero, J. *J. Mol. Struct.* **1994**, *328*, 297–323. (d) Grech, E.; Klimkiewicz, J.; Nowicka-Scheibe, J.; Pietrazak, M.; Schilf, W.; Pozharski, A. F.; Ozeryanskii, V. A.; Bolvig, S.; Abildgaard, J.; Hansen, P. E. *J. Mol. Struct.* **2002**, *615*, 121–140, and references cited therein.

(13) For recent reviews, see: (a) Brown, S. P.; Spiess, H. W. *Chem. Rev.* **2001**, *101*, 4125–4155. (b) Reichert, D. *Annu. Rep. NMR Spectrosc.* **2005**, *55*, 159–203. (c) Eckert, H.; Elbers, S.; Epping, J. D.; Janssen, M.; Kalwei, M.; Strojek, W.; Voigt, U. *Top. Curr. Chem.* **2005**, *246*, 195–233. (d) Ashbrook, S. E.; Smith, M. E. *Chem. Soc. Rev.* **2006**, *35*, 718–735. (e) Brown, S. P. *Prog. Nucl. Magn. Reson.* **2007**, *50*, 199–251, and references cited therein.

(14) (a) Harris, R. K.; Jackson, P.; Merwin, L. H.; Say, B. J.; Hagele, G. *J. Chem. Soc., Faraday Trans.* **1988**, *84*, 3649–3649. (b) Harris, R. K. *Solid State Sci.* **2004**, *6*, 1025–1037. (c) Taulelle, F. *Solid State Sci.* **2004**, *6*, 1053–1057. (d) Harris, R. K. *Analyst* **2006**, *131*, 351–373.

(15) For some selected recent publications, see: (a) Geen, H.; Titman, J. J.; Gottwald, J.; Spiess, H. W. *Chem. Phys. Lett.* **1994**, *227*, 79–86. (b) Gottwald, J.; Demco, D. E.; Graf, R.; Spiess, H. W. *Chem. Phys. Lett.* **1995**, *243*, 314–323. (c) Brown, S. P.; Schaller, T.; Seelbach, U. P.; Koziol, F.; Ochsenfeld, C.; Kläner, F.-G.; Spiess, H. W. *Angew. Chem.* **2001**, *113*, 740−743; *Angew. Chem., Int. Ed.* **2001**, *40*, 717−720. (d) Ochsenfeld, C.; Brown, S. P.; Schnell, I.; Gauss, J.; Spiess, H. W. *J. Am. Chem. Soc.* **2001**, *123*, 2597–2606. (e) Ochsenfeld, C.; Kussmann, J.; Koziol, F. *Angew. Chem.* **2004**, *116*, 4585−4589; *Angew. Chem., Int. Ed.* **2004**, *43*, 4485−4489. (f) Brown, S. P.; Lesage, A.; Elena, B.; Emsley, L. *J. Am. Chem. Soc.* **2004**, *126*, 13230–13231. (g) Densmore, C. G.; Rasmussen, P. G.; Goward, G. R. *Macromolecules* **2005**, *38*, 416–421. (h) Alam, T. M.; Nyman, M.; McIntyre, S. K. *J. Phys. Chem. A* **2007**, *111*, 1792–1799. (i) Schaller, T.; Büchele, U. P.; Kläner, F.-G.; Bläser, D.; Boese, R.; Brown, S. P.; Spiess, H. W.; Koziol, F.; Kussmann, J.; Ochsenfeld, C. *J. Am. Chem. Soc.* **2007**, *129*, 1293–1303, and references cited therein.

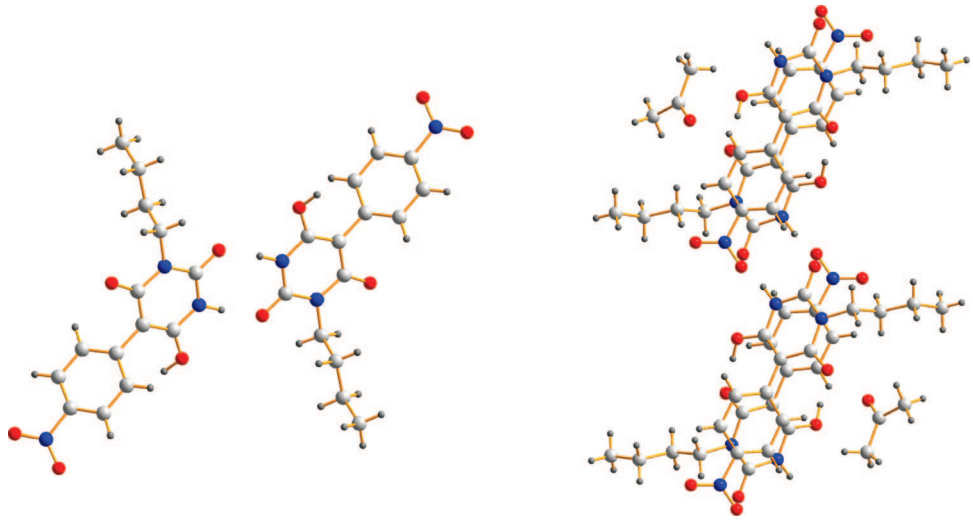

FIGURE 1. Molecular structure of dimeric **1** and projection along the *b*-axis showing the packing of the barbiturate molecules and acetone. Note that the orientation of the OH-protons is fixed due to hydrogen-bonding to a carbonyl group of a symmetry-produced neighboring **1** molecule.

in solids could be obtained by 1D (single-quantum, SQ) ^{1}H magic-angle spinning (MAS) NMR and 2D homonuclear dipolar double-quantum (DQ) techniques.[13a,e,15] In such a two-dimensional experiment, double-quantum coherences due to pairs of dipolar coupled protons are correlated with single-quantum coherences resulting in characteristic correlation peaks. Double-quantum coherences between *like* spins appear as a single correlation peak on the diagonal while a pair of cross peaks that are symmetrically arranged on either side of the diagonal reflect couplings among *unlike* spins. In addition, we exploit the fact that observable DQ signal intensities are proportional to D_{ij}^2 or r_{ij}^{-6}, respectively (D_{ij} is the homonuclear dipolar coupling constant, r_{ij} the internuclear distance). Strong signal intensities in the corresponding double-quantum spectrum therefore reveal protons in rather close spatial proximity (e.g., distances up to 3.5 Å). Protons involved in hydrogen-bonded structures typically exhibit well-resolved ^{1}H chemical shifts, mainly between 8 and 20 ppm, thereby providing valuable structural information. Since in solid compounds ^{1}H chemical shifts are also affected by subtle packing arrangements, e.g., stacking of aromatic moieties,[16] the interpretation of experimental data may be facilitated by comparison with density functional theory (DFT)[17] based *ab initio* chemical shift calculations. Furthermore, the molecular assemblies of **1** with **PS** and **DAC** were studied by means of differential scanning calorimetry (DSC) and UV/vis spectroscopy.

II. Results and Discussion

Solid-State NMR Results, Quantum Chemical Calculations, and X-ray Analyses. Crystallographic Data of the Barbiturate 1. After recrystallization from acetone tiny single-crystals of **1** suitable for X-ray analysis were obtained. It was found that **1** crystallizes in a monoclinic lattice, space group $P2_1/c$ (No. 14), with the lattice parameters $a = 11.3856(5)$ Å, $b = 7.8718(4)$ Å, and $c = 19.8518(6)$ Å. The asymmetric unit consists of two molecules: one molecule **1** and one acetone molecule. Two molecules of **1** are linked together by symmetric and strong hydrogen bonds between the respective C═O and NH groups of the barbituric acid moieties yielding a centrosymmetric dimer rather typically found for barbiturates[18] (Figure 1).

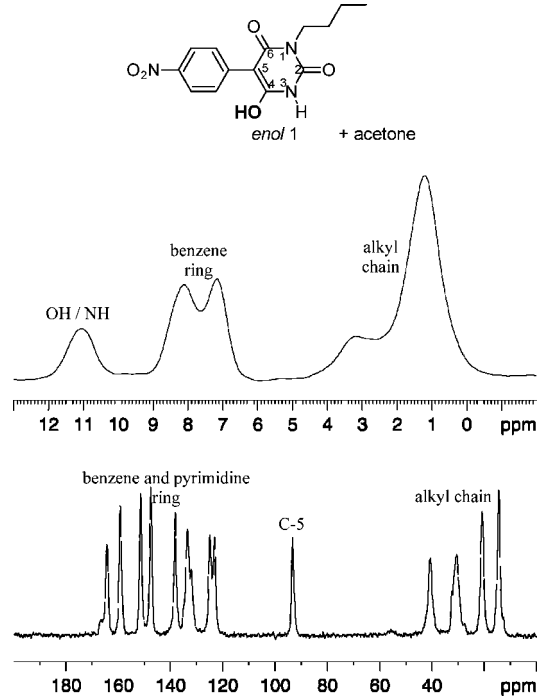

FIGURE 2. ^{1}H MAS NMR (top) and ^{13}C CP MAS NMR spectrum of **1** (bottom). The tiny peak at 55 ppm indicates a minor impurity of *keto*-type structure of **1**. The broadening of the peak at 30 ppm is due to overlapping signals (methyl groups of acetone and alkyl chains of **1**).

Solid-State NMR Spectra of 1. An inspection of the ^{13}C CP MAS NMR spectrum of **1** lacks evidence for the presence of a methine carbon (expected at about 55 ppm) suggesting an *enol*-type structure for **1** (Figure 2). This finding is reminiscent of a previous study on Schiff bases derived from 5-aminobar-

(16) (a) Wasserfallen, D.; Fischbach, I.; Chebotavera, N.; Kastler, M.; Pisula, W.; Jäckel, F.; Watson, M. D.; Schnell, I.; Rabe, J. P.; Spiess, H. W.; Müllen, K. *Adv. Funct. Mater.* **2005**, *15*, 1585–1594. (b) Brown, S. P.; Schnell, I.; Brand, J. D.; Müllen, K.; Spiess, H. W. *Phys. Chem. Chem. Phys.* **2000**, *2*, 1735–1745.

(17) Parr, R. G., Yang, W. *Density Functional Theory of Atoms and Molecules*; Oxford University Press: Oxford, 1989.

(18) Allen, F. H. *Acta Crystallogr.* **2002**, *B58*, 380–388.

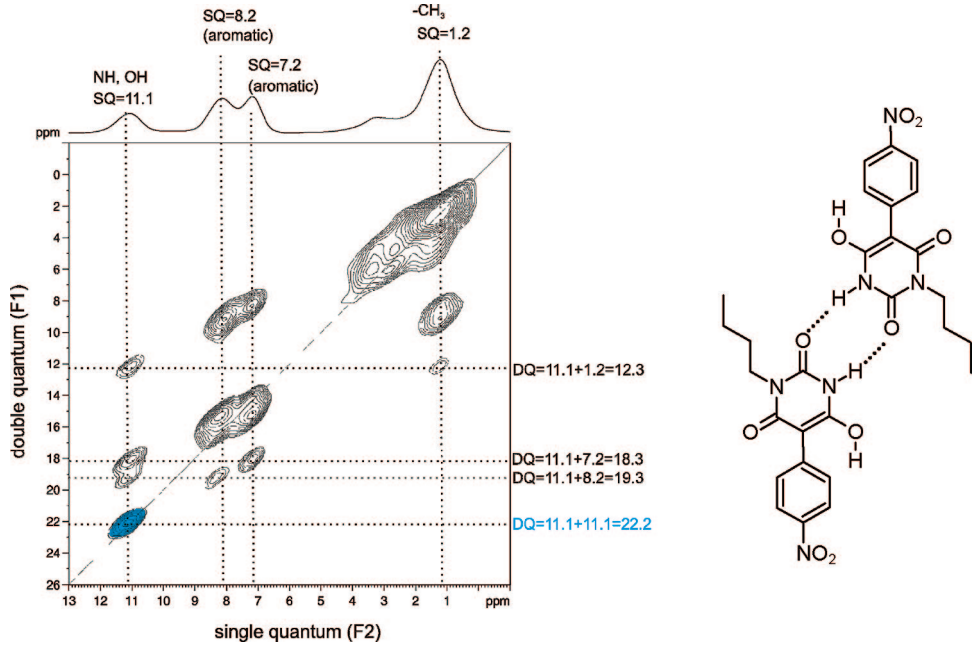

FIGURE 3. ^{1}H−^{1}H DQ MAS NMR spectrum of **1** at 850 MHz and 59524 Hz MAS, acquired under the following experimental conditions: $\tau_{(exc.)}$ = 33.6 μs, 256 t_1 increments at steps of 16.8 μs, relaxation delay 5 s, 32 transients per increment. Sixteen positive contour levels between 4% and 62% of the maximum peak intensity were plotted. The F_2 projection is shown on the top.

TABLE 1. Influence of the Chemical Environment on the Chemical Shifts δ in ppm of 1 and Its Molecular Assemblies with the Proton Sponge PS and 2,6-Diacetamidopyridine DAC, and Combination thereof Observed by ^{1}H MAS NMR Spectroscopy[a]

	1	**1**+DAC	**1**+PS	**1**+PS+DAC
barbiturate **1**				
enol-NH	11.1 (10.2)	11.2 (12.5)		
enol-OH	11.1 (4.3)	12.3 (5.3)		
enolate-NH			10.6 (10.5)	10.2 (11.4)
DAC-NH		10.7, 9.7		11.8, 9.9
		(11.0, 10.3)		(12.6, 10.9)
PS-NH$^+$			18.0 (19.2)	19.3 (19.2)

[a] Computed ab initio ^{1}H chemical shifts are given in parentheses.

bituric acid, where the *enol* form appeared to be more stable than the *keto* form.[9b] Notably, the ordering of the alkyl chains strongly depends on the (re)crystallization conditions (e.g., crystallization rate, polarity of the solvent used). While slow crystallization from diethyl ether and subsequent recrystallization from dichloromethane yields substantially disordered alkyl chains (e.g., revealed as noticeable splitting of the aliphatic ^{13}C signals, see the Supporting Information), crystallization from acetone produces highly ordered alkyl chains (cf. crystal structure, Figure 1).

Since in solution a rapid equilibration between both the *keto* and *enol* forms of the enolizable barbiturate **1** occurs, it is important to distinguish the two possible *enol* structures in the solid-state (cf. Scheme 1). In that context, the influence of the respective morphology (single crystal vs polycrystalline powder) on the crystallochromic properties of **1** is addressed. A wide range of crystallographically different properties, such as polymorphism, the ability of a compound to crystallize in more than one crystal structure,[19] phase transitions, and molecular reorientation of alkyl chains,[20] are known within the barbiturate family and thus may complicate the structure refinement.

The ^{1}H MAS NMR spectrum of **1** reveals one high-frequency shifted proton peak at 11.1 ppm, reflecting that the respective protons (NH and OH) are indeed involved in hydrogen-bonding. In order to allow for an assignment of the hydrogen-bonded protons, we acquired a ^{1}H−^{1}H DQ MAS NMR spectrum of **1** at a rather short dipolar recoupling time ($2\tau_R$ = 33.6 μs, Figure 3). According to the crystal structure, the distance of the two NH-protons within the dimer amounts to d = 2.5283 Å (D_{ij} = 7.43 kHz), while the OH-proton has longer distances to aromatic protons (d = 2.9154 Å, D_{ij} = 4.85 kHz) as well as to methyl protons of acetone (d = 2.9657 Å, D_{ij} = 4.61 kHz). In contrast, the NH-protons have larger distances to both aromatic (d = 3.3829 Å, D_{ij} = 3.1 kHz) and aliphatic protons (d = 3.5561 Å, D_{ij} = 2.67 kHz). Since the dipolar couplings among the protons are very sensitive with respect to the distance (cf. static dipolar couplings D_{ij} given in parentheses), this should be reflected by the observed DQ signal intensities. The presence of a strong DQ peak at 22.2 ppm (11.1 ppm + 11.1 ppm) suggests that it originates from NH-protons that are involved in dimer formation. This is also supported by the rather weak cross peak at 19.3 ppm (11.1 ppm + 8.2 ppm) reflecting the contact of the NH-protons with aromatic protons. However, the fairly strong DQ cross peaks at 18.3 ppm (11.1 ppm + 7.2 ppm (aromatic)) and 12.3 ppm (11.1 + 1.2 ppm (aliphatic)) indicate that the proton peak at 11.1 ppm also contains the OH-protons. All observed DQ peaks (and their respective signal intensities) are in qualitative agreement with expectations from the given crystal structure. Nevertheless, the spectral data does not reveal a clear preference of *enol*1- vs *enol*2-type structure in the solid compound **1**. In that respect, we have to refer to the crystal structure, which contains *enol*1-type molecules of **1**. In cases

(19) (a) Cleverley, B.; Williams, P. P. *Tetrahedron* **1959**, *7*, 277–288. (b) Craven, B. M.; Vizzini, E. A. *Acta Crystallogr.* **1969**, *B25*, 1993–2009. (c) Craven, B. M.; Vizzini, E. A. *Acta Crystallogr.* **1971**, *B27*, 1917–1924. (d) Caillet, J.; Claverie, P. *Acta Crystallogr.* **1980**, *B36*, 2642–2645. (e) Craven, B. M.; Fox, R. O., Jr.; Weber, H.-P. *Acta Crystallogr.* **1982**, *B38*, 1942–1952. (f) Lewis, T. C.; Tocher, D. A.; Price, S. L. *Cryst. Growth Des.* **2004**, *4*, 979–987. (g) Lewis, T. C.; Tocher, D. A.; Price, S. L. *Cryst. Growth Des.* **2005**, *5*, 983–993.

(20) (a) Nichol, G. S.; Clegg, W. *Acta Crystallogr.* **2005**, *B61*, 464–472. (b) Nichol, G. S.; Clegg, W. *Acta Crystallogr.* **2005**, *C61*, o297–o299.

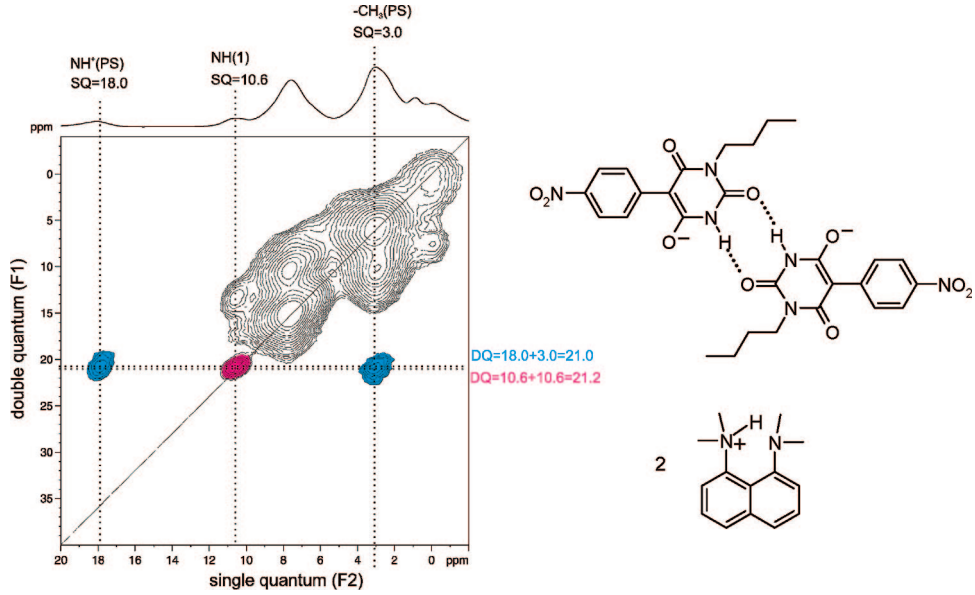

FIGURE 4. ^{1}H−^{1}H DQ MAS NMR spectrum of **1**+**PS** at 700 MHz and 29762 Hz MAS, acquired under the following experimental conditions: $\tau_{(exc.)} = 33.6\ \mu s$, 128 t_1 increments at steps of 33.6 μs, relaxation delay 5 s, 16 transients per increment. Sixteen positive contour levels between 4% and 63% of the maximum peak intensity were plotted. The F_2 projection is shown on the top. The strong (NH/NH) correlation peak at 21.2 ppm (10.6 ppm + 10.6 ppm) indicates the persistence of the dimeric structure of the *enolate* anion of **1** reflecting the stability of this arrangement.

where the experimentally observed ^{1}H MAS NMR line shapes are solely broadened by strong homonuclear dipolar couplings among abundant protons, high-resolution ^{1}H MAS spectra can in principle be obtained using so-called homonuclear dipolar decoupling sequences like windowed phase-modulated Lee−Goldburg (wPMLG)[21,21b] or windowed DUMBO-1[21c] that also constitute the key part of high-resolution DQ spectra (DQ-CRAMPS[15f]). However, this approach requires a rather high degree of local order or crystallinity which is quite difficult to achieve for a bulk NMR sample of **1**.

Acid−Base Behavior of 1. To evaluate the stability of the dimeric unit in **1** with respect to bases, we treated the barbiturate **1** with the so-called Proton Sponge (1,8-bis(dimethylamino)-naphthalene, **PS**). Proton sponges show both high thermodynamic basicity and slow *inter*molecular proton transfer kinetics[12a–c] and thus facilitate complete deprotonation of **1**. Indeed, the ^{1}H MAS NMR spectrum of **1**+**PS** exhibits a high-frequency shifted resonance at 18.0 ppm that we attributed to a chelated proton[12a] resulting from acid−base reaction of **PS** and the more acidic OH-proton of **1**, while the NH-proton resonates at 10.6 ppm. This assignment is backed up by ab initio DFT chemical shift calculations, where the chemical shifts of both the chelated proton and the NH-proton of the *enolate* anion are computed at 19.2 and 10.5 ppm, respectively (cf. Table 1). Notably, the corresponding ^{1}H−^{1}H DQ MAS NMR spectrum (Figure 4) of **1**+**PS** not only shows a strong DQ cross peak at 21.0 ppm (18.0 ppm + 3.0 ppm) between the chelated proton and the methyl protons of the Proton Sponge but also a strong DQ correlation peak among the NH-protons at 21.2 ppm (10.6 ppm + 10.6 ppm). Based on this, the deprotonation of **1** appears rather complete. The aromatic and aliphatic proton signals of both the Proton Sponge and **1** strongly overlap and, hence, yield no further insight into the dipolar coupled proton network. Taken together, the DQ spectrum of **1**+**PS** is consistent with a dimeric arrangement of the *enolate* anion of **1**. This behavior is quite expected since **PS** does *not* possess a molecular recognition sequence suitable for selective binding to an ADA sequence offered by the *enolate* anion. A similar packing arrangement is reported for the complex of barbituric acid with **PS** whereas **PS** cations are orientated in separate $\pi-\pi$ stacks.[22] However, the change in ^{1}H chemical shift of the NH-proton of $\Delta\delta = -0.5$ ppm suggests a slight stretching of the NH---O═C hydrogen bond within the *enolate* dimer.[23]

Hydrogen-Bonding Ability. The complex formation of the barbiturate **1** and its *enolate* anion in **1**+**PS** is investigated with the adenine-mimetic base 2,6-diacetamidopyridine **DAC** offering a complementary hydrogen-bonding pattern to the *keto*1/*keto*2 and *enol*2 structure(s) of **1** as well as to the *enolate* anion. It is anticipated that the dimer of **1** or its *enolate* anion will be broken while forming a hydrogen-bonded complex of **1**+**DAC** or **1**+**PS**+**DAC**. In particular, we are interested in the expected reorientation of the self-aggregated *enol*1-type **1** to a complementary ADA sequence.

The ^{1}H MAS NMR spectrum of the complex **1**+**DAC** (recrystallized from acetone) is rather complicated and exhibits exchangeable proton sites at 16.8, 16.5, 12.3, 11.2, 10.7, and 9.7 ppm, respectively. It is noteworthy to mention that the two NH-protons in pure **DAC** resonate at 9.4 ppm and 10.7 ppm (see the Supporting Information). To elucidate the complex structure and to facilitate an assignment of the various peaks, we acquired a ^{1}H−^{1}H DQ MAS NMR spectrum. Notably, we found *no* so-called *auto*-correlation peaks (diagonal peaks) among the exchangeable protons, suggesting that the former dimer of the barbiturate **1** is broken. Rather, a new complex **1**+**DAC** was formed revealing itself via characteristic cross peaks (Figure 5). Assuming that the resonance at 11.2 ppm can be assigned to the NH-proton of **1**, the cross peaks at 21.9 ppm

(21) (a) Leskes, M.; Madhu, P. K.; Vega, S. *J. Chem. Phys.* **2008**, *128*, 052309/1–052309/11. (b) Leskes, M.; Madhu, P. K.; Vega, S. *J. Chem. Phys.* **2006**, *125*, 124506/1–124506/18. (c) Lesage, A.; Sakellariou, D.; Hediger, S.; Elena, B.; Charmont, P.; Steuernagel, S.; Emsley, L. *J. Magn. Reson.* **2003**, *163*, 105–113.

(22) Nichol, G. S.; Clegg, W. *Cryst. Growth Des.* **2006**, *6*, 451–460.

(23) Harris, R. K.; Phuong, Y.; Robert, B.; Ma, C. Y.; Roberts, K. J. *Chem. Commun.* **2003**, 2834–2835.

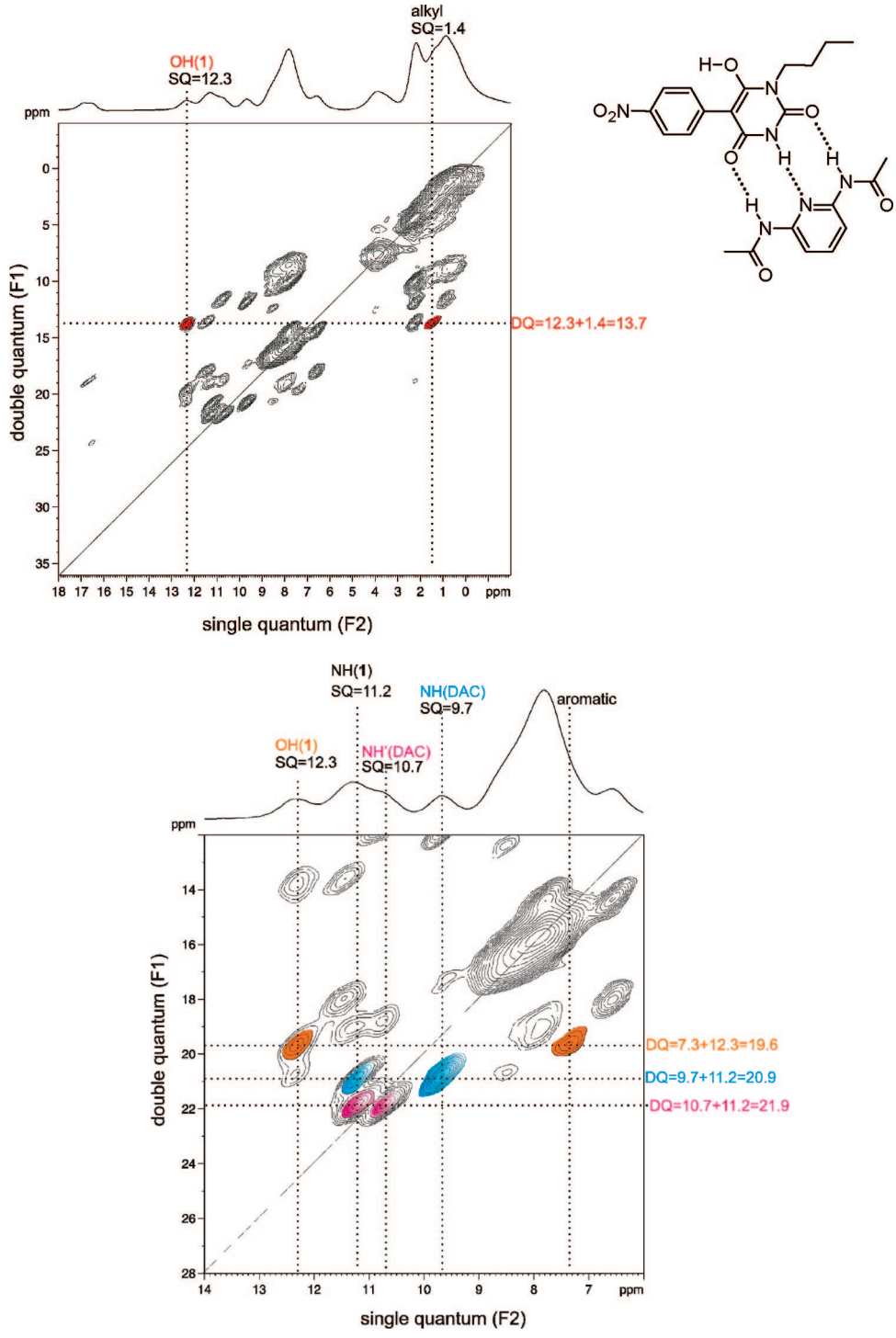

FIGURE 5. ^{1}H−^{1}H DQ MAS NMR spectrum of **1**+**DAC** at 850 MHz and 59524 Hz MAS, acquired under the following experimental conditions: $\tau_{(exc.)} = 33.6$ μs, 256 t_1 increments at steps of 16.8 μs, relaxation delay 10 s, 32 transients per increment. Sixteen positive contour levels between 2% and 35% of the maximum peak intensity were plotted. The F_2 projections are given. (Top) Full spectrum. (Bottom) Excerpt highlighting the important OH/NH cross peaks.

(11.2 ppm + 10.7 ppm) and 20.9 ppm (11.2 ppm + 9.7 ppm) indicate complexation of **1** with **DAC**, as they reflect close contacts of the NH-proton of **1** with the two NH-protons of **DAC**. Their comparable signal intensities hint at very similar distances of the **1**-NH-proton to the two **DAC**-NH-protons. The rather small peaks at 16.8 ppm and 16.5 ppm, respectively, are assigned to protons from a 2,6-diacetamidopyridinium cation **DAC-H**$^+$, thus suggesting that a minor fraction of the **1**+**DAC** undergoes an acid−base reaction. In addition, the OH-proton resonance of **1** is assigned based on its DQ cross peak at 19.6 ppm (12.3 ppm + 7.3 ppm) with adjacent aromatic protons.

Two possible structures of an anticipated complex **1**+**DAC** have been obtained from ab initio geometry optimizations. Indeed, the rather simple molecular approach cannot account for solid-state packing effects possibly present in the compound, but nevertheless, the computed chemical shifts (cf. Table 1) are good enough to support the assignment of the NH-peaks in the corresponding ^{1}H MAS NMR spectrum. In the case of vicinal

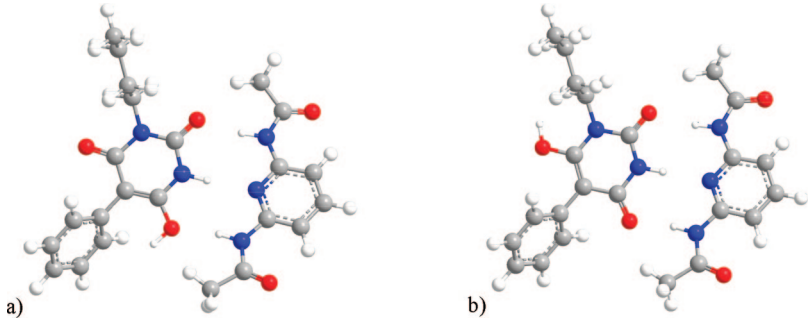

FIGURE 6. Optimized model geometries of **1**+**DAC**: (a) assuming *enol*1-type **1** and (b) *enol*2-type **1** after tautomeric rearrangement. Both structures and the NMR chemical shieldings have been obtained at BLYP/6-311++G(2df,2pd) and B3LYP/6-311++G(2df,2pd) levels of theory, respectively, using Gaussian03. NMR chemical shifts were computed with respect to tetramethyl silane (TMS).

NH and OH protons of **1** (cf. Figure 6a), the two NH-protons of **DAC** were computed at 11.0 and 8.7 ppm, respectively, while the **1**-NH-proton is predicted at 12.4 ppm. The OH-proton is computed at 7.3 ppm and, thus, clearly reflects that the optimized model geometry is only a rough snapshot of the actual structural arrangement. The initially given model geometry of **1**(*enol*1)+**DAC** (Figure 6a) is based on the assumption that the barbituric acid moiety possibly retains its *enol*1-type structure and indeed predicts fairly close contact of the **1**-OH-proton to one of the **DAC**-NH protons (d = 2.892 Å, D_{ij} = 5.0 kHz). In that case, we would expect a strong DQ cross peak at 23.0 ppm (12.3 ppm + 10.7 ppm), which is *not* observed in the corresponding DQ spectrum (cf. Figure 5). Rather, the OH-proton has a fairly strong DQ peak at 13.7 ppm (12.3 ppm + 1.4 ppm) indicating contact to the alkyl chain protons of **1**. This strongly suggests that the OH-proton is of *enol*2-type within the complex **1**+**DAC**, thus hinting at a tautomeric rearrangement of **1** upon complexation as illustrated in Figure 6b. In this case, an optimized model geometry of **1**(*enol*2)+**DAC** yields computed proton chemical shifts of 12.5 ppm (**1**-NH) as well as 11.0 ppm and 10.3 ppm, respectively, for the two **DAC**-NH-protons. In addition, the **1**-OH-proton is computed at 5.3 ppm. Notably, the **1**-OH proton shows close contact to the aliphatic protons of **1** (d = 1.827 Å, D_{ij} = 19.7 kHz), which is in rather good agreement with the experimental data.

Adding the adenine-mimetic base 2,6-diacetamidopyridine **DAC** to the system **1**+**PS**, we offer a complementary hydrogen-bonding pattern to the *enolate* anion of **1**, which indeed should allow for complex formation.

After recrystallization from acetone, orange needle-like single-crystals suitable for X-ray analysis were obtained. It was found that **1**+**PS**+**DAC** crystallizes in a monoclinic lattice, space group $P2_1/n$ (No. 14), with the lattice parameters a = 8.9840(5) Å, b = 17.4356(7) Å, and c = 23.5112(8) Å. The asymmetric unit consists of an *enolate* **1**+**DAC** complex and one molecule **PS** with a chelated proton that populates both $N(CH_3)_2$ units of **PS** in a 50:50 ratio. The *enolate* complex **1**+**DAC** is stabilized by hydrogen bonds between the C=O/N and NH groups of both **DAC** and **1**.

In the solid-state ^{1}H MAS NMR spectrum of the mixture **1**+**PS**+**DAC**, four different exchangeable proton sites are resolved at 19.3 (chelated proton), 11.8, 10.2, and 9.9 ppm, respectively. The formation of the *enolate* anion of **1** in the presence of **PS** is evidenced by a strong DQ cross peak at 21.7 ppm (19.3 ppm + 2.4 ppm) between the chelated proton (19.3 ppm) and the methyl protons of **PS** (2.4 ppm) in the corresponding ^{1}H−^{1}H DQ MAS NMR spectrum (Figure 8). Notably, there is no *auto*-correlation peak of the NH-protons of **1** which

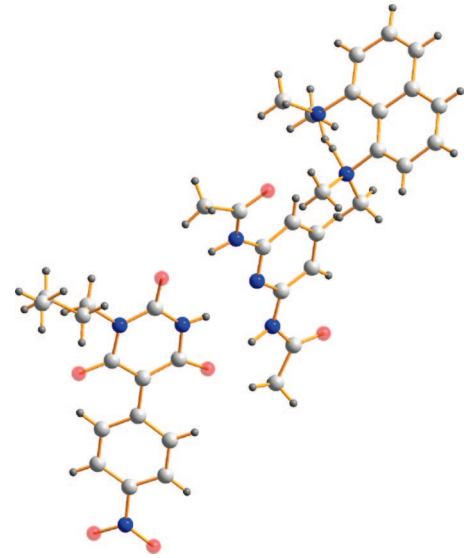

FIGURE 7. Molecular structure of the hydrogen-bonded complex of **DAC** with the *enolate* anion of **1** in the presence of **PS** (asymmetric unit). Note that the chelated proton **PS**-H^+ populates the two $N(CH_3)_2$ units at a 50:50 ratio.

implies that the former dimer of the *enolate* anions in **1**+**PS** is canceled. Assuming that the **1**-NH-proton can be assigned to the peak at 10.3 ppm, both DQ cross peaks at 22.0 ppm (11.8 ppm + 10.3 ppm) and 20.2 ppm (9.9 ppm + 10.3 ppm), respectively, indicate successful formation of an *enolate* **1**+**DAC** complex fulfilling the complementary hydrogen-bonding pattern. This observation is indeed consistent with the crystal structure. Again, an analysis of proton−proton distances within 4 Å facilitates an unambiguous peak assignment: the crystallographically different **DAC**-NH-protons are in closest contact to the **1**-NH-proton (d = 2.4669 Å, D_{ij} = 8.0 kHz and d = 2.6242 Å, D_{ij} = 6.6 kHz, respectively). In addition, four contacts of **1**-NH to aromatic protons of both **PS** (d = 3.1624 Å, D_{ij} = 3.8 kHz; d = 3.2184 Å, D_{ij} = 3.6 kHz) and **DAC** (d = 3.3725 Å, D_{ij} = 3.1 kHz; d = 3.4594 Å, D_{ij} = 2.9 kHz), respectively, are found in the crystal structure, which are reflected by a rather weak DQ cross peak at 17.6 ppm (10.2 ppm + 7.4 ppm), but *no* contact to aliphatic protons (also not observed in the DQ spectrum, Figure 8). In contrast, the two **DAC**-NH-protons have shortest contacts to the methyl protons of **DAC** (d = 2.0139 Å, D_{ij} = 14.7 kHz; d = 2.0051 Å, D_{ij} = 14.9 kHz), which is reflected by strong DQ cross peaks at 12.8 ppm (11.8 ppm + 1.0 ppm) and 11.6 ppm (9.9 ppm + 1.7 ppm).

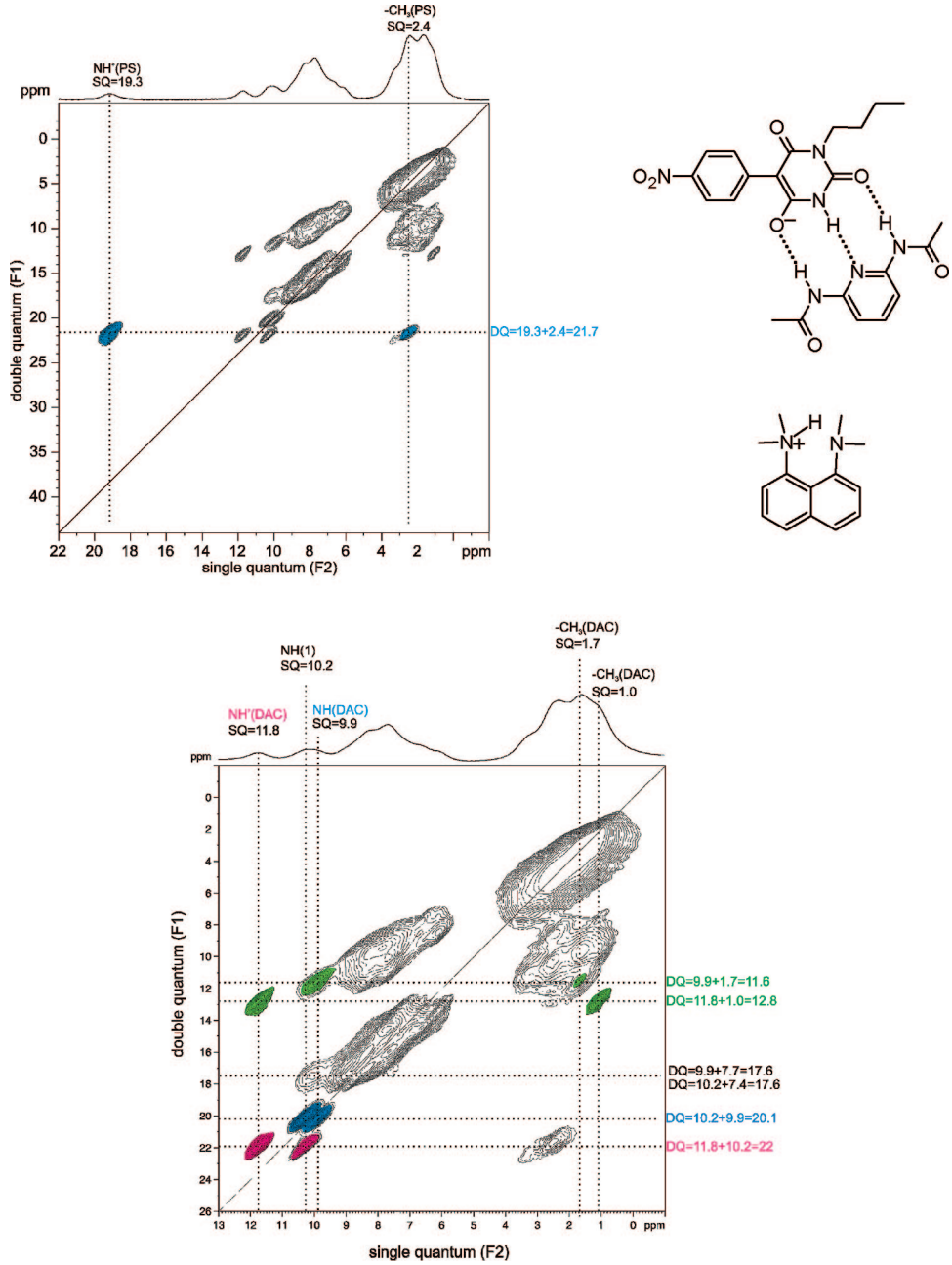

FIGURE 8. ^{1}H−^{1}H DQ MAS NMR spectrum of **1**+**PS**+**DAC** at 850 MHz and 59524 Hz MAS, acquired under the following experimental conditions: $\tau_{(exc.)} = 33.6\ \mu$s, 256 t_1 increments at steps of 16.8 μs, relaxation delay 10 s, 32 transients per increment. Sixteen positive contour levels between 7% and 95% of the maximum peak intensity were plotted. The F_2 projections are given. (Top) Full spectrum. (Bottom) Excerpt highlighting the important NH/NH cross peaks.

On the other hand, corresponding distances of the **DAC**-NH-protons to aromatic protons are much larger ($d = 3.2953$ Å, $D_{ij} = 3.3$ kHz; $d = 3.4446$ Å, $D_{ij} = 2.9$ kHz), thus resulting in a considerably weaker DQ cross peak at 17.4 ppm (9.9 ppm + 7.5 ppm). The second DQ cross peak of aromatic protons involving the **DAC**-NH-proton at 11.8 ppm is missing and hence suggests that the distance between two dipolar coupled protons at the given DQ excitation period of 33.6 μs is limited to about 3.3 Å. In summary, the DQ spectrum of **1**+**PS**+**DAC** is in perfect agreement with the reported crystal structure. While **DAC** may act as a weak base in the mixture **1**+**DAC** yielding a minor fraction of **1**-*enolate*, the presence of the much stronger base **PS** clearly allows for complete removal of the **1**-OH-proton and thus, **DAC** is solely involved in complex formation with **1**.

An inspection of Table 2 reveals that the hydrogen bond lengths within the various assemblies are strongly affected by the presence of the Proton Sponge. While the barbiturate NH-resonances in pure **1** as well as in the complex **1**+**DAC** are

(24) (a) Tsiourvas, D.; Sideratou, Z.; Haralabakopoulos, A. A.; Pistolis, G.; Paleos, C. M. *J. Phys. Chem.* **1996**, *100*, 14087–14092. (b) Yang, W.; Chai, X.; Tian, Y.; Chen, S.; Cao, Y.; Lu, R.; Jiang, Y.; Li, T. *Liq. Cryst.* **1997**, *22*, 579–583. (c) Würthner, F.; Yao, S.; Heise, B.; Tschierske, C. *Chem. Comm.* **2001**, 2260–2261. (d) Itahara, T.; Uto, T.; Sunose, M.; Ueda, T. *J. Mol. Struct.* **2002**, *616*, 213–220. (e) Hao, X.; Liang, C.; Jian-Bin, C. *Analyst* **2002**, *127*, 834–837. (f) Sivakova, S.; Rowan, S. J. *Chem. Commun.* **2003**, 2428–2429.

TABLE 2. Experimental or Calculated Intermolecular Distances of 1 and Its Molecular Assemblies with PS and DAC

compound	bond type	distances D^a (Å)	distances d^b (Å)
1[a]	N−H---O═C	2.7725	1.8263
1+**DAC**[c]	**1**-C═O---HN-**DAC**	3.032	2.016
	1-C═O---H′N-**DAC**	2.971	1.952
	1-NH---N-**DAC**	3.075	2.031
1+**PS**+**DAC**[a]	**1**-C═O---HN-**DAC**	2.9405	1.9903
	1-C═O---H′N-**DAC**	2.7893	1.8385
	1-NH---N-**DAC**	3.0444	2.2033

[a] N---O, N---N, and O---O distances are directly obtained from single-crystal X-ray data. [b] Hydrogen bond lengths (the hydrogen atoms were refined with respect to known geometries using SHELXS86[30] software). [c] Data obtained from an ab initio structure assuming *enol*2-type **1**.

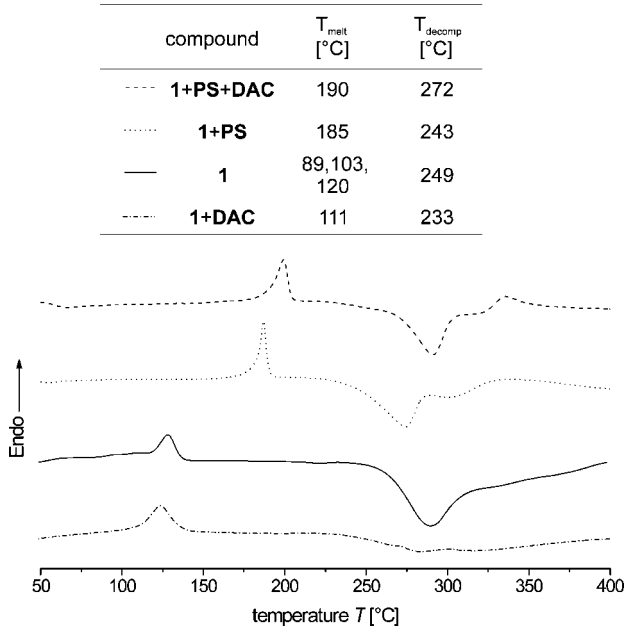

FIGURE 9. DSC thermograms of the complex **1**+**DAC** and **1**+**PS**+**DAC** in comparison with the starting compounds **1** and **1**+**PS**. Inset: comparison of the observed onset temperature for the melting (T_{melt}) and decomposition (T_{decomp}).

almost identical (11.1 vs 11.2 ppm) indicating comparable hydrogen bond lengths, a removal of the OH-proton and, thus, formation of an *enolate* anion due to acid−base reaction with **PS** results in a high-field shift of NH-resonances in both dimeric *enolate* anion of **1**+**PS** (**1**-NH: 10.6 ppm) and in the **DAC**-complexed *enolate* anion of **1**+**PS**+**DAC** (**1**-NH---N-**DAC**, 10.2 ppm) possibly reflecting local changes of electron delocalization. Indeed, rather strong interaction of the **DAC**-NH′-proton with the *enolate* oxygen (**1**-C−O$^-$---H′N-**DAC**) is evidenced by the change in ^{1}H chemical shift of the **DAC**-NH′-proton of $\Delta\delta = +1.1$ ppm with respect to pure **DAC** and a shorter hydrogen bond length than observed in the complex **1**+**DAC**.

DSC Thermograms of the Barbiturate 1 and of the Corresponding Structures with PS and DAC. Calorimetric investigations are very useful tools for the determination of thermal stability of compounds. Indeed, complex formation may be concluded from DSC (differential scanning calorimetry) traces by displacements of corresponding phase transitions. Well-organized supramolecular structures are observed at higher transition temperatures, whereas lower or else broader transition temperatures indicate destabilized packing effects of the added receptor to the molecular structure of the host.[24] The DSC traces of the complex **1**+**DAC** and **1**+**PS**+**DAC**, respectively, in comparison with the starting compounds **1** and **1**+**PS** are shown in Figure 9.

The DSC thermogram of **1** shows two negligible endothermic peaks at 89 and 103 °C hinting at evaporating acetone. The endothermic transition at 120 °C is attributed to the melting of barbiturate **1**, while the exothermic at 249 °C indicates decomposition. In contrast, a sample recrystallized from diethyl ether (see the Supporting Information) shows two intense endothermic transitions at 107 and 127 °C. There, the first peak reflects molecular reorientation of the *n*-butyl chain[20] revealing disorder of the alkyl chains in this sample. Upon addition of **DAC** to the barbiturate **1**, a lower and broader melting peak (111 °C) and decomposition temperature (233 °C) of **1**+**DAC** is observed suggesting that the former hydrogen-bonded dimeric arrangement of **1** is broken. Notably, *no* evidence for unbound **1** or **DAC** was found in this sample (recrystallized from acetone), which is in contrast to the crude product obtained from diethyl ether (Et_2O).

The salt **1**+**PS** shows an endothermic melting peak at 185 °C and an exothermic peak at 243 °C indicating decomposition. The stabilizing effect of the adenine-mimetic base **DAC** to the *enolate* anion of **1** in the complex **1**+**PS**+**DAC** is revealed by a broader and higher endothermic phase transition at 190 °C (probably due to an eutectic behavior of the *enolate* anion of **1** with **DAC**) and a higher exothermic peak at 262 °C (decomposition).

Taken together, the DSC-investigations prove that all compounds are thermally stable up to 100 °C and thus, any possible frictional heating effects during fast MAS NMR experiments (60 kHz spinning) can safely be neglected.

Push−Pull Character of 1 and in Its Molecular Assemblies Investigated by Solid-State UV/vis Spectroscopy. In the previous parts, we have presented the molecular structure of the enolic barbiturate **1** and its molecular assemblies with the Proton Sponge **PS** and 2,6-diacetamidopyridine **DAC**, and combination thereof. In this last section, we elucidate the observed UV/vis response (Scheme 2, Figure 10) of the chromophoric **1** caused by the molecular recognition, thus demonstrating the versatile bonding potential of this new type of compound. The structural details derived from solid-state NMR spectroscopy are in good agreement with the corresponding UV/vis absorption bands of all assemblies.

The UV/vis absorption band of the single-crystals of **1** has its maximum at 414 nm. Due to the presence of acetone in the crystal structure, the polarity of the environment is increased which significantly enhances the push−pull character of the *enol*1-type **1**. Shoulders at approximately 440 and 470 nm are probably resulting from a charge-transfer excitation. For comparison, the crude product of **1** obtained from Et_2O absorbs at 334 nm. Furthermore, the solvent used for recrystallization remarkable influences the position of the complex formation equilibrium. For example, the complexation of **1** with **DAC** from Et_2O is incomplete which demonstrates that the hydrogen-bonded dimer of *enol*1-type **1** is fairly stable in Et_2O (see the Supporting Information). In contrast, recrystallization of the complex **1**+**DAC** from acetone results in a clear UV/vis absorption maximum at 425 nm. In comparison to pristine **1** from acetone, the bathochromic shift ($\Delta\lambda = 11$ nm, $\Delta\tilde{\nu} = 625$ cm^{-1}) of the UV/vis absorption band is attributed to the

SCHEME 2. Influence of the Hydrogen-Bonded Structures of the Complex 1+DAC and 1+PS+DAC in Comparison with the *Enol*1-Type 1 and Its *Enolate* Anion in 1+PS on the UV/vis Absorption Band of the Chromophor

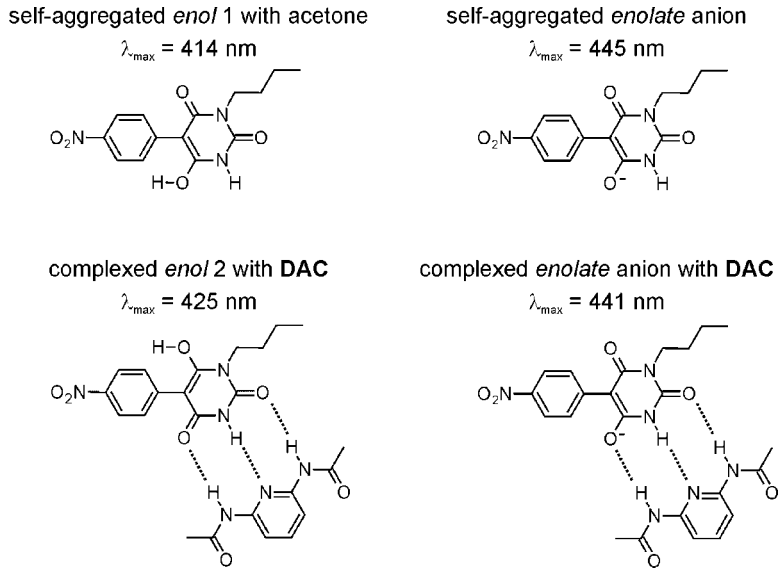

hydrogen bond between the NH-proton of *enol*2-type **1** and the electron-rich ring nitrogen of **DAC** increasing the electron density of the barbituric acid moiety. Another support for this interpretation is the broken stacked arrangements of **1** which has decreased the (+)M-effect of the barbiturate. This feature is of importance for our conceptual development of a novel type of adjustable UV/vis probe for detection of supramolecular sequences.

Quantitative proton-transfer between **1** and **PS** is verified by the observation of a single UV/vis absorption band at 445 nm representing self-aggregated *enolate* anion of **1** (cf. Figure 4). Due to the deprotonation, the electron-donating effect of the barbituric acid moiety in the *enolate* anion is increased yielding a significant bathochromic shift ($\Delta\lambda = 34$ nm, $\Delta\tilde{\nu} = 1683$ cm^{-1}) in the UV/vis spectrum of **1**+**PS** compared to **1**from acetone. In the complex **1**+**PS**+**DAC** the electron density of the *enolate* oxygen is decrease due to the hydrogen bond to the NH proton of **DAC** (cf. Scheme 2). So, the decrease of the (+M)-effect of the *enolate* oxygen involved in complex formation with **DAC** is noticed by a small hypsochromic shift ($\Delta\lambda = 4$ nm, $\Delta\tilde{\nu} = 204$ cm^{-1}) of the UV/vis absorption band in comparison to **1**+**PS**.

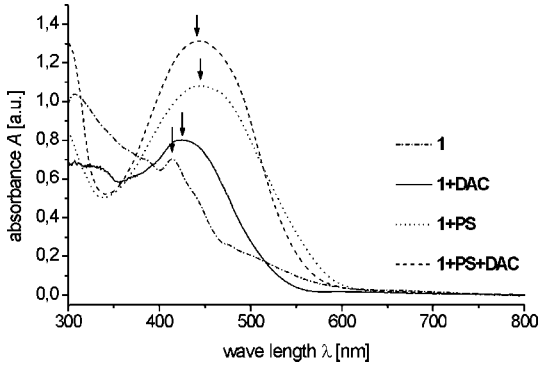

FIGURE 10. Solid-state UV/vis spectra of the complex **1**+**DAC** and **1**+**PS**+**DAC** in comparison to the starting compound **1** and **1**+**PS**. For structure assignment to the UV/vis response, see Scheme 2.

III. Conclusions

The novel enolizable chromophor 1-*n*-butyl-5-(4-nitrophenyl)barbituric acid **1** displays adjustable hydrogen-bonding properties. In the solid-state, an *enol* form with a DDA hydrogen-bonding pattern is preferred that self-aggregates to hydrogen-bonded dimers. These dimers are involved in stacked arrangements stabilized by additional hydrogen bonds. In the presence of strong bases like the so-called Proton Sponge **PS**, a simple acid−base reaction occurs where the OH-proton of **1** is stripped. The corresponding *enolate* anion of **1** retains the dimeric structure reflecting the stability of this arrangement. It was found that the *enolic* dimer of **1** can be broken upon addition of the adenine-mimetic base 2,6-diacetamidopyridine **DAC**, which provides a complementary DAD hydrogen-bonding. The solvent used for (re)crystallization highly influences the equilibrium of complex formation. In particular for **1**+**DAC**, complex formation is strongly preferred using the solvent acetone, while otherwise self-aggregation of **1** is observed to compete with complex formation. Furthermore, complexation with **DAC** induces the molecular reorientation of **1** to the complementary ADA sequence. This nicely demonstrates that both the prototropic tautomerism and the acidity of the enolizable barbituric acid **1** in the solid compounds is strongly influenced by ordering or packing effects, which are absent in solution-state. The corresponding solid-state structures were characterized using both X-ray analysis and solid-state NMR spectroscopy. Interpretation of the obtained NMR data was supported by DFT-based ab initio chemical shift calculations. Depending on the chemical environment, complementary information on crystallochromic properties of **1** and its derivatives were revealed by UV/vis spectroscopy measured in diffuse reflection. It was shown that the electron-donating strength of the barbituric acid moiety is significantly influenced by interaction with bases. Therefore, this type of enolizable barbituric acid derivatives is a promising candidate to measure effects of complementary hydrogen-bonded complexes as well as the basicity of the environment by means of UV/vis spectroscopy.

IV. Experimental Section

Synthesis of 1-*n*-Butyl-5-(4-nitrophenyl)barbituric Acid 1. 4.0 mmol of 1-*n*-butyl-5-phenylbarbituric acid was dissolved in 3 mL concentrated sulfuric acid, cooled off 0 °C, and then treated with 5.0 mmol of powdery KNO_3 over a time period of 5 min. After continuously stirring for 30 min at the same temperature, the reaction mixture was allowed to warm up at 22 °C. To complete the reaction, the mixture was stirred for 2 h again and then poured into 5 mL of ice−water. The precipitate was filtered off, washed with water (4 × 3 mL), and dried in vacuo. The powdery crude product was washed with a small amount of dichloromethane (DCM) and recrystallized from diethyl ether (Et_2O). After drying under reduced pressure (40 °C, 40 mbar), **1** was obtained as a pale yellow precipitate. Yield: 19 %. Mp: 107, 127, 262 °C (decomp.). MS (ESI): *m*/*z* calcd for $C_{14}H_{16}N_3O_5$ ($M + H^+$) 306.2860, found 306.1504. IR (cm^{-1}): 3200−3000 (w), 2965, 2934, 2873 (m), 1707 (s), 1617, 1597 (m), 1542 (m), 1518 (s), 1457 (m), 1345 (s), 1109 (w), 857 (m), 781 (m), 598 (m). ^1H NMR (DCM-d_2): 0.93 (t, 3 H, CH_3), 1.33 (se, 2 H, CH_2), 1.58 (quin, 2 H, CH_2), 3.89 (t, 2 H, N-CH_2), 4.82 (s, 1 H, 5), 7.46 (d, 2 H, 2′), 8.25 (d, 2 H, 3′), 8.52 (s, 1 H, NH-3). ^{13}C NMR (DCM-d_2): 13.5 (CH_3), 20.0 (CH_2), 29.9 (CH_2), 41.8 (N-CH_2), 55.0 (5), 124.2 (3′), 130.0 (2′), 139.6 (1′), 148.1 (4′), 149.5 (2), 165.4 (4/6), 166.3 (6/4). Anal. Calcd for $C_{14}H_{15}N_3O_5$: C, 55.08; H, 4.95; N, 13.76. Found: C, 55.28; H, 4.70; N, 13.71.

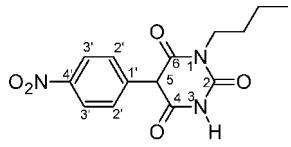

keto-**1**

The crystal structure of **1** discussed in the paper was obtained by slow recrystallization from acetone. Mp: 89, 103, 120, 249 °C (decomp.). ^1H NMR (DCM-d_2): 0.93 (t, 3 H, CH_3), 1.34 (m, 2 H, CH_2), 1.59 (m, 2 H, CH_2), 2.12 (s, 6 H, acetone), 3.89 (t, 2 H, N-CH_2), 4.81 (s, 1 H, 5), 7.47 (d, 2 H, 2′), 8.17 (s, 1 H, NH-3), 8.25 (d, 2 H, 3′). ^1H NMR (acetone-d_6): 0.91 (t, 3 H, CH_3), 1.35 (m, 2 H, CH_2), 1.58 (m, 2 H, CH_2), 3.85 (dt, 2 H, N-CH_2), 5.27 (s, 1 H, 5), 7.70 (d, 2 H, 2′), 8.27 (d, 2 H, 3′), 10.47 (s, 1 H, NH-3). Anal. Calcd for $C_{14}H_{15}N_3O_5 + C_3H_6O$: C, 56.19; H, 5.83; N, 11.56. Found: C, 55.80; H, 5.90; N, 11.49.

Solid-State NMR Methods. Proton solid-state NMR data was recorded on either a 850 or 700 MHz spectrometer; additional ^{13}C CP MAS NMR spectra were recorded at 75.5 MHz using a 500 MHz machine. Most experiments were carried out using a 1.3 mm double-resonance MAS probe at a spinning frequency of 60 kHz, typical $\pi/2$-pulse lengths of 2 μs, and recycle delays of 5−10 s. Additional spectra were acquired using 2.5 mm double-resonance MAS probe at spinning frequencies of 30 kHz. The spectra are referenced with respect to tetramethyl silane (TMS) using adamantane as secondary standard (1.86 ppm for ^1H and 29.46 ppm for ^{13}C). If not stated otherwise, all spectra were collected at room temperature. The back-to-back (BaBa) recoupling sequence was used to excite and reconvert double-quantum coherences,[25] applying the States-TPPI method[26] for phase-sensitive detection. Further details are given in the figure captions of the respective 2D-spectra.

DFT-Based Chemical Shift Calculations. Where necessary, equilibrium geometries of the investigated compounds were obtained by density functional theory (DFT)[17] based quantum chemical calculations using the BLYP functional[27] and 6-311G[28] split valence basis set augmented with diffuse and polarization functions. Subsequently, ^{13}C chemical shifts with respect to tetramethyl silane (TMS) were computed at B3LYP/6-311++G (2df, 2pd) level of theory with the GIAO approach as implemented in Gaussian03 program.[29]

Single-Crystal Structure Analyses. (a) Crystal parameters of **1** are reported as follows: pale yellow; $C_{17}H_{21}N_3O_6$; $M_r = 363.77$; monoclinic $P2_1/c$; $a = 11.3856(5)$ Å, $b = 7.8718(4)$ Å, $c = 19.8518(6)$ Å; $\beta = 91.114(1)°$; $Z = 4$. (b) Crystal parameters of **1**+**PS**+**DAC** are reported as follows: orange needles; $C_{29}H_{35}N_5O_4$; $M_r = 570.24$; monoclinic $P2_1/n$; $a = 8.9840(5)$ Å, $b = 17.4356(7)$ Å, $c = 23.5112(8)$ Å; $\beta = 97.33(0)°$; $Z = 5$. In both cases, data collection was carried out at 120 K (Mo Kα ($\lambda = 0.71073$ Å)) equipped with a graphite monochromator. Intensity data were corrected for Lorentz and polarization effects. Structure solution and refinement was done employing the SHELXS86[30] and CRYSTALS[31] software packages. All non-hydrogen atoms were refined in the anisotropic approximation against F of all observed reflections. The hydrogen atoms were refined in the riding mode with fixed isotropic temperature factors; (**1**): $R = 0.066$; (**1**+**PS**+**DAC**): $R = 0.1522$. The figures were created using the Diamond 3.1b[32] program package.

DSC Analyses. Calorimetric melting profiles were determined in the temperature range from 25 to 400 °C (scan rate of 10 °C min^{-1}) in a stream of nitrogen.

UV/vis Spectroscopy. The UV/vis absorption spectra of the solid-state compounds were obtained by means of a diode-array spectrometer in diffuse reflection. The measurements were carried out in the spectral range of 180−1000 nm using quartz plates and Spectrolon as the standard white reference.

Acknowledgment. Financial support from the DFG (Deutsche Forschungsgemeinschaft) through the SFB 625 in Mainz is gratefully acknowledged.

Supporting Information Available: Synthetic procedures, general experimental methods, optimized geometries, CIF files, spectral data not shown in the manuscript, as well as a complete ref 29. This material is available free of charge via the Internet at http://pubs.acs.org.

JO800598Z

(25) (a) Sommer, W.; Gottwald, J.; Demco, D. E.; Spiess, H. W. *J. Magn. Reson.* **1995**, *A 113*, 131–134. (b) Feike, M.; Demco, D. E.; Graf, R.; Gottwald, J.; Hafner, S.; Spiess, H. W. *J. Magn. Reson.* **1996**, *A122*, 214–221. (c) Saalwächter, K.; Graf, R.; Spiess, H. W. *J. Magn. Reson.* **1999**, *140*, 471–476. (d) Saalwächter, K.; Graf, R.; Spiess, H. W. *J. Magn. Reson.* **2001**, *148*, 398–418.

(26) Marion, D.; Ikura, M.; Tschudin, R.; Bax, A. *J. Magn. Reson.* **1989**, *85*, 393–399.

(27) (a) Becke, A. D. *Phys. Rev. A* **1988**, *38*, 3098–3100. (b) Lee, C.; Yang, W.; Parr, R. G. *Phys. Rev. A* **1988**, *37*, 785–789.

(28) Krishnan, R.; Binkley, J. S.; Seger, R.; Pople, J. A. *J. Chem. Phys.* **1980**, *72*, 650–654.

(29) Frisch, M. J. *Gaussian 03 Revision D.02*; Gaussian, Inc.: Wallingford, CT, 2004. The complete reference is available in the Supporting Information.

(30) Sheldrick, G. M. *SHELXS-86, Program package for crystal structure solution and refinement*; Univeristät Göttingen: Germany, 1986.

(31) Betteridge, P. W.; Carruthers, J. R.; Cooper, R. I.; Prout, K.; Watkin, D. J. *J. Appl. Crystallogr.* **2003**, *36*, 1487.

(32) Brandenburg, K., *DIAMOND 3.1b*; Crystal Impact: Bonn, Germany, 2006.